ACCEPTED MANUSCRIPT
LIMA, José; FARIA, Paulina; SANTOS SILVA, António - Earth Plasters: The Influence of Clay Mineralogy in the Plasters' Properties. International Journal of Architectural Heritage. ISSN 1558-3066. (2020), p. 1–16. doi: 10.1080/15583058.2020.1727064.
Available at: https://www.tandfonline.com/doi/full/10.1080/15583058.2020.1727064

Earth Plasters: The Influence of Clay Mineralogy in the Plasters' Properties

José Lima[a]*, Paulina Faria[b,c], and António Santos Silva[d]

[a]*Faculty of Architecture, University of Lisbon, Lisbon, Portugal;* [b]*CERIS, Civil Engineering Research and Innovation for Sustainability, Instituto Superior Técnico, Lisbon, Portugal;* [c]*Department of Civil Engineering, Faculty of Science and Technology, NOVA University of Lisbon, Caparica, Portugal;* [d]*Department of Materials, National Laboratory for Civil Engineering, Lisbon, Portugal*

*corresponding author: José Lima, Faculty of Architecture, University of Lisbon, Rua Sá Nogueira, 1349-055, Lisboa, Portugal. Email: jose.lima.ferreira@gmail.com

Abstract: Earth-based mortars have been used all over the world since ancient times in an extensive range of building types from vernacular architecture to monuments. Plastering is one of the most common contemporary applications of earth-based mortars used for earthen-building conservation or modern architecture. Raw earth is a very diverse natural material, and clay minerals play a key role in plaster properties being responsible for their setting process and providing the capacity of balancing the indoor hygrometric conditions of buildings. This capacity offers significant benefits to energy savings delivering comfort and health of inhabitants and also contributes to building conservation. For this study, three mortars were produced with different clayish earths to assess the influence of clay mineralogy. Mortars characterization confirmed that clay mineralogy drives important plaster properties, such as vapour adsorption and drying shrinkage, while also having a significant influence on mechanical strength, dry abrasion, and thermal conductivity. Within the studied mortars, illitic clayish earth stands outs as more adequate for earth-based plasters, showing balanced properties, namely linear drying shrinkage, mechanical strength, dry abrasion, and water vapour adsorption.

Keywords: clayish earth; drying shrinkage; hygroscopicity; illitic clay; kaolinitic clay; montmorillonitic clay; mortar characterization; pore size distribution: vapour adsorption; water erosion

1. Introduction

Earth-based mortar was probably the first type of mortars to be used by humankind when ancestors mixed excavated earth with water to fill the space between wood branches used to build shelters. Thereafter, earth-based mortars have been used all over the world as masonry layering mortar or as wall, ceiling, and floor protective or decorative coatings in an extensive range of building types, from vernacular architecture to monuments (Bruno et al. 2010; Schroeder 2016).

Each earth is a natural raw material characterized by its own and unique properties due to its diverse composition comprising certain types and content ratios of clay, silt, sand, and gravel. Therefore, earth-based mortar properties are highly dependent on the type of earth used (Minke 2006; Schroeder 2016). Nowadays, plastering is one of the main applications of earth-based mortars for which raw earth is disaggregated and sieved to remove gravel. If the content of clay is too high, sand (or other artificial aggregate with similar particle size distribution) must be added to control shrinkage. For this purpose, a recurrent proportion between the fine particles of earth (clay and silt) and sand is 1:3 in volume, with water addition of 20-30% in weight of the dry components (Emiroğlu, Yalama, and Erdoğdu 2015; Lagouin et al. 2019; Lima, Faria, and Santos Silva 2016).

Clay minerals play a key role in this type of mortars being responsible for its setting process, associated only with drying unless a binder is added for chemical stabilization, as well as, when used for plastering, its contribution to the equilibrium of indoor hygrometric conditions due to clay minerals' high hygroscopicity (Maskell et al. 2018; Santos, Nunes, and Faria 2017; White and Borrelli 1959). Montmorillonitic clays are known for having very high hygroscopicity and very high shrinkage. Kaolinitic clays, on the other hand, are recognized for the opposite: low shrinkage and low hygroscopicity. Illitic clays normally present average conditions with a compromise between shrinkage and hygroscopicity. Although these effects

are referred in the literature (Bergaya and Lagaly 2013; Murray 2007), to the authors' knowledge they were not yet quantified when the clays are used to produce plasters or its influence on the properties and durability of those plasters.

Earth-based mortars have specific characteristics in comparison to conventional binder mortars, such as cement-based or lime-based mortars. To the authors' awareness, the only standard specifically dedicated to defining requirements, classification, and test procedures for earth mortar is the German standard DIN 18947 (DIN 2013), which was followed in the present study. For some of the tests this DIN standard refers to several parts of EN 1015 standards that will be addressed further ahead.

This study aims to assess the influence of earths with different clays upon the properties of earth-based plasters. Thus, three mortars were produced with three different clayish earths, each containing a clay with prevalence of a specific clay mineral, namely either a montmorillonitic clay, a kaolinitic clay, or an illitic clay. All mortars were formulated considering the same volumetric ratio of clayish earth and siliceous sand.

Mortar mixing, fresh state characterization, as well as sample preparation and hardened state characterization, including drying shrinkage, bulk density, thermal conductivity, dynamic modulus of elasticity, compressive, flexural and adhesive strengths, and dry abrasion, were performed. As earth mortars are vulnerable to water, hardened state characterization also included water absorption by capillarity and drying behaviour, water erosion by dripping action, dynamic water vapour adsorption and desorption, and pore size distribution. Results are presented and compared between the different clayish earth-based plasters to results obtained with other plasters from previous studies. The influence of each of the clays is highlighted as to the advantages and disadvantages of eco-efficient plaster applications.

2. Materials and methods

2.1. Materials

The three types of clayish earth used to prepare the mortars assessed in this study were extracted from three different locations in Portugal where the predominant clay minerals were assessed in previous studies. The illitic clayish earth (E) was extracted from a clay quarry located in the eastern part of Algarve region in southern Portugal and was previously studied (Lima and Faria 2016; Lima, Faria, and Santos Silva 2016). This sector of the Algarve's sedimentary basin presents a high concentration of reddish soils with a mineralogy dominated by the illite clay mineral (Manuppella et al. 1985; Trindade et al. 2013). After open air drying, the illitic clayish earth was mechanically ground to pass through a 2 mm sieve. The kaolinitic clay (K) was supplied by the Mibal mining company and was quarried from the Barqueiros deposit located near Barcelos city in the northwestern region of Portugal. This sedimentary deposit is characterized by the presence of highly concentrated kaolinitic layers, showing extremely fine grains and colour variations ranging from extreme whiteness to shades of yellow (Mibal 2005; Santos et al. 2014). The raw material was supplied in powder form ground to pass through a 30 μm sieve. The montmorillonitic clayish earth (B) was extracted from Serra de Dentro region in Porto Santo Island in the Madeira archipelago where small size deposits of greenish-yellowish bentonite clay occur due to the submarine alteration process of pyroclastic volcanic rock of trachyte composition (Cordeiro et al. 2010). After open air drying, the raw earth was mechanically ground to pass through a 2 mm sieve. The sand used for the formulation of all mortars assessed in this study, labelled S, is a siliceous unwashed sand extracted from a quarry located in Santiago do Cacém in the southwest part of Portugal.

2.2. Methods

2.2.1. Mineralogical characterization

The mineralogical characterization of the three clayish materials used in the present study was confirmed through X-ray diffraction analysis (XRD) complemented by thermogravimetric and differential thermal analysis (TG-DTG). XRD was obtained with a Phillips PW3710 X-ray diffractometer using Fe-filtered Co Kα radiation with 35 kV and 45 mA and speed of 0.05 º/s ranging from 3 to 74º 2θ. The crystalline phases were identified by matching them to the International Centre for Diffraction Data Powder Diffraction Files (ICDD PDF). The TG-DTG tests were performed in a Netzsch STA 449 F1 analyzer under nitrogen atmosphere with a heating rate of 10 °C/min from room temperature to 1000 °C.

2.2.2. Loose bulk density and particle size distribution

The loose bulk density of the clayish materials and the sand was determined based on EN 1097–3 (CEN 1998c). The particle size distribution of the sand S was analysed by dry sieving, according to standard EN 1015–1 (CEN 1998a).

2.2.3. Mortars formulation and fresh state characterization

The three earth-based mortars were formulated considering the same volumetric proportions of clayish earth and siliceous sand, respectively, 1:3. For each mortar one of the previously mentioned clayish earth was used, namely the illitic clayish earth for mortar labelled E1S3, kaolinitic clay for mortar labelled K1S3, and montmorillonitic clayish earth for mortar labelled B1S3.

The standard DIN 18947 (DIN 2013) was followed for preparing and mixing the mortars as well as for fresh state characterization. Mortars E1S3 and K1S3 were prepared with the minimum amount of water required to ensure adequate workability and compliance with the

flow table consistency defined in the DIN 18947 (175 ± 5 mm). To prepare mortar B1S3, due to thixotropic behaviour of the montmorillonitic clay, the amount of water used was the minimum to guarantee adequate workability. Although presenting flow table consistency under the minimum limit defined in the DIN 18947 (DIN 2013), the workability of the mortar was considered excellent. The mortar formulation is reported in Table 1, in terms of both volumetric and weight percentages of clayish earth, sand, and water contents. Wet density determined by EN 1015–6 (CEN 1998b) and flow table consistency, assessed according to EN 1015–3 standard (CEN 1999a), are also reported.

Table 1. Composition and fresh state mortar characterization.

	Volumetric proportions					Weight proportions						
	E	K	B	S	Water (a)	E	K	B	S	Water (b)	Density (c)	Consistency (d)
Mortar	[%]	[%]	[%]	[%]	[%]	[%]	[%]	[%]	[%]	[%]	[kg/m^3]	[mm]
E1S3	25.0	0.0	0.0	75.0	19.6	21.6	0.0	0.0	78.4	12.8	2130.7	173.2
K1S3	0.0	25.0	0.0	75.0	22.3	0.0	7.6	0.0	92.4	17.2	2028.0	170.4
B1S3	0.0	0.0	25.0	75.0	31.3	0.0	0.0	18.3	81.7	21.3	1957.8	165.2

Notation: E – Illitic clayish earth (muscovite); K, Kaolinitic clay; B, Montmorillonitic clay (bentonite); S, siliceous unwashed sand; (a) percentage of volume added, considering the total volume of clayish earth and sand; (b) percentage of mass added, considering the total mass of clayish earth and sand; (c) fresh state density; (d) flow table consistency.

2.2.4. Samples preparation

Mortar samples preparation also followed the DIN 18947 (DIN 2013). Six prismatic samples of 160 mm x 40 mm x 40 mm were prepared in metallic moulds to test each mortar as to linear drying shrinkage, dry bulk density, dynamic modulus of elasticity, and flexural and compressive strength. These samples were demoulded after drying. Adhesive strength and dry abrasion resistance were assessed on samples of 20 mm plaster layer applied over hollow bricks with a surface of approximately 295 mm x 195 mm simulating a plaster, thus allowing three and four tests per sample, respectively. For testing thermal conductivity, six circular samples of 90 mm diameter and 20 mm thickness were used moulded in cylindrical PVC moulds. Three

planar samples, with a surface area of 1000 cm² (500 mm x 200 mm) and a thickness of 15 mm, were prepared for each mortar in a metallic mould and kept in it for testing.

Specimens were prepared from some of these samples to perform other tests. Their preparation is presented further ahead along with the test procedure description.

2.2.5. Common hardened state characterization

The mortars were evaluated as to linear drying shrinkage (DIN 2013), dry bulk density (CEN 1999b), dynamic modulus of elasticity (CEN 2004), flexural and compressive strength (CEN 1999c), adhesive strength (CEN 2000), dry abrasion resistance (DIN 2013), as well as thermal conductivity, performed with a Heat Transfer Analyzer ISOMET 2104 with a 60 mm diameter contact probe API 210412 with a measurement range of 0.3 to 2.0 W/(mK).

2.2.6. Dynamic vapour adsorption and desorption

For the dynamic adsorption and desorption test, the DIN 18947 (DIN 2013) was followed. The samples were kept in the metallic moulds during testing to guarantee that vapour adsorption and desorption would occur only in the top exposed surface.

The samples were stabilized in a climatic chamber at 50% relative humidity (RH) and 23 ºC. After the stabilization of the samples, the climatic chamber condition was set to 80% RH for the adsorption test phase. The samples were weighed at time intervals defined on the standard, respectively: 0, 1, 3, 6, and 12 h. An exception was made for the 0.5 h defined weighing which was suppressed to minimize the interference of the climatic chamber stabilization time associated with the weighing process. The adsorption test was extended until 24 h, beyond the 12-h interval defined in the standard to achieve a more comprehensive understanding of the adsorption behaviour of the samples. After 24 h, the samples were weighted and the condition of the chamber was changed back to 50% RH forcing the samples

to a desorption phase, which was assessed with the same time interval protocol during another period of 24 h.

2.2.7. Water absorption by capillarity action and drying behaviour

The water absorption by capillarity action test followed the standard EN 15801 (CEN 2009) with some adaptions due to the specific characteristics of the analysed earth-based mortar – their vulnerability to liquid water. Three specimens from each mortar were cut from the prismatic samples, with 40 mm × 40 mm × 40 mm. The sawn surface of the specimens was cleaned by compressed air and was chosen for the determination of water absorption by capillarity. The lateral surfaces of the specimens were waterproofed with a mixture of equal portions of colophony resin and beeswax, applied melted at approximately 90 °C. After the waterproofing of the lateral surfaces the specimens were dried to constant mass in a ventilated oven at a temperature of 60 ± 5 °C. Before the first weighing and the beginning of the test the specimens were allowed to stabilize to room temperature.

Since earth-based mortars, when in direct contact with water, become plastic over a short period, it is impossible to handle the specimens directly during the long testing period. To overcome this issue, test baskets were prepared to carry each specimen during the test. The baskets were designed specifically to minimize the amount of water retained in the basket during the consecutive weighing process and to maintain it as constant as possible, which needed to be accounted for in the test results. The side walls of the test basket were made out of a plastic squared tube with a section of 75 mm × 75 mm cut at a height of 40 mm (Figure 1A). The bottom base of the basket was constructed from a fine aluminium mesh with mesh spacing of approximately 1.8 mm (Figure 1B). The bottom base aluminium mesh was fashioned over the plastic element and affixed with aluminium tape, positioned offset from the edge of the plastic element by at least 5 mm to avoid water retention under the tape during the test due to capillary action (Figure 1C). To minimize the loss of fine particles, that might detach from

the earthen specimens during the consecutive weighing process, a very fine polyethylene mesh fabric (Figure 1D) was placed inside each basket prior to the introduction of the specimen (Figure 1E) to act as a fine particle filter during the testing procedure (Figure 1F).

The test was carried in a controlled environment room (T = 20.2 ± 0.8 °C and RH = 55 ± 6.0%) in a test chamber with saturated humid environment to minimize evaporation during the test. Before the beginning of the test, each basket was dry weighed with the polyethylene filter in place. The amount of water to be retained by each set during the test was estimated by the difference of the mean of six wet weightings to the set dry weight. The overall baskets mean retained water was 0.12 g, with a standard error of 0.02 g (mean of each basket standard deviation).

The test starts when the dry specimens placed inside the baskets (with the polyethylene filter) are put in the flat tank try over a saturated bedding layer made by a capillary medium (equivalent to "Vileda Wetex" composed by natural fibres, respectively, 70% cellulose and 30% cotton). During the test, the water in the tank tray is periodically refilled to guarantee each basket and specimen set are immersed from 1 to 2 mm. In the first 5 min of the test, the specimens are weighed at 1 min intervals, then weighed at 5 min intervals until the 30 min time has lapsed. From that point forward, the specimens are weighed at 1, 2, 3, 6, and 24 h and, from then on, again weighed at 24 h intervals until the end of the test, which occurs when the difference between two successive weighing (24 h) is not greater than 1% of the mass of water absorbed by the specimen. The weight of the absorbed water per unit of the water-exposed surface area was reported (in kg/m^2) as a function of the square root of time (in $min^{0.5}$), allowing to determine the capillary water absorption coefficient (AC), corresponding to the slope of the most representative aligned segments of the capillarity curve representative of mortar capillary behaviour.

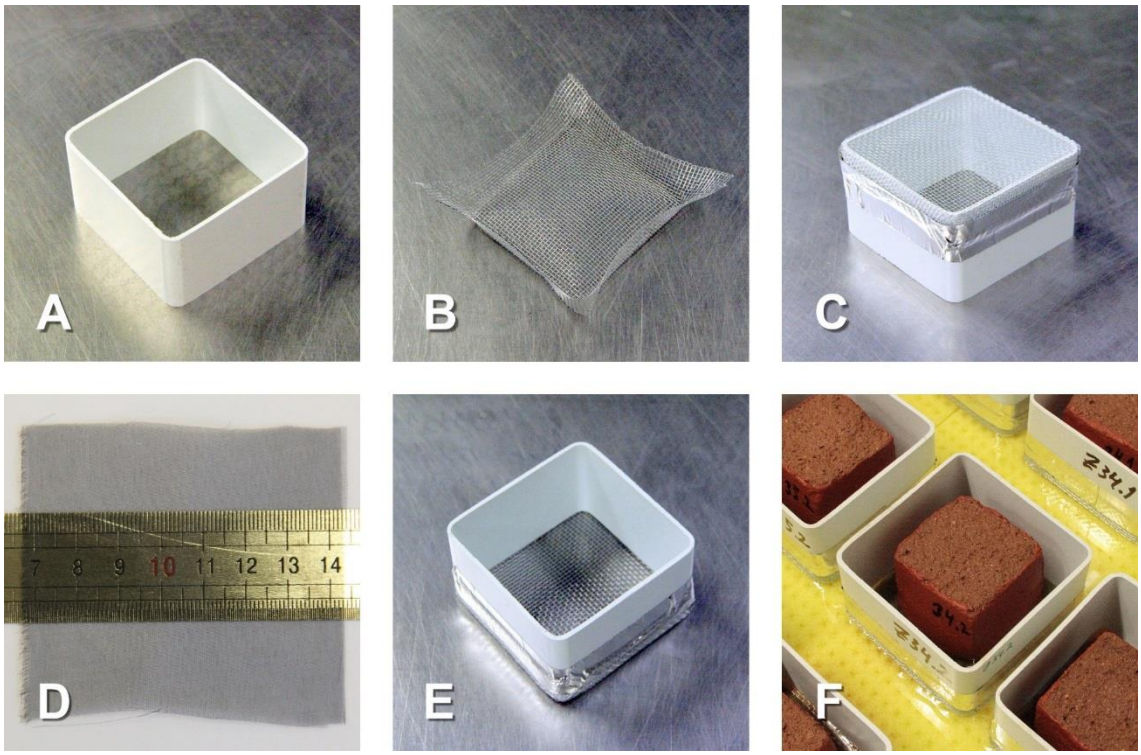

Figure 1. Specific test basket assembly: (A) plastic squared tube with a section of 75 mm × 75 mm, cut with a height of 40 mm, for basket side walls; (B) fine aluminium mesh, with mesh spacing of approximately 1.8 mm, for basket bottom base; (C) bottom base aluminium mesh, fixed to the plastic element with aluminium tape, with an offset from the edge of at least 5 mm; (D) very fine polyethylene mesh fabric used as a fine particle filter; (E) prepared test basket with the polyethylene filter inside; (F) specimens in the baskets over the polyethylene filter during testing.

The drying behaviour test had begun immediately after the end of the water absorption by capillarity action test, therefore, with the specimens in a full saturation condition. The procedure followed the standard EN 16322 (CEN 2013) with adaptions due to the specific characteristics of the analysed earth-based mortars. Because the saturated specimens could not be handled directly, they were kept inside the basket sets during the drying test. To guarantee that the evaporation process occurred only through the specimen top surface, each basket set was placed in an individual flat plate previously dry weighed. The test was carried in the same controlled environment room (T = 20.2 ± 0.8 °C and RH = 55 ± 6.0%). In the first hour the specimens were weighed with 10 min interval, then weighed at 2, 3, 6, and 24 h, and from then on weighed

at intervals of 24 h until the end of the test reached when the specimens achieve equilibrium with the room environmental conditions defined as two successive weighing (24 h) with a difference not greater than 0.1%. The residual amount of water present in the specimen per unit of the evaporation surface area (in kg/m²) was reported as a function of the time (in h) to allow the assessment of the drying rate of the first drying phase (D_1) and as a function of the square root of the time (in $h^{0.5}$) to determine the rate of water vapour diffusion of the second drying phase (D_2).

2.2.8. Water erosion by dripping action

The test methodology to evaluate the plaster resistance to water erosion by dripping action was adapted from the erosion test (Geelong method) defined in the New Zealand Standard NZS 4298:1998/A1 (NZS 2000). This NZS standard was developed to test rammed earth samples, adobe, or pressed earthen blocks with specific dimensioned for the test (300 mm × 300 mm × 125 mm). According to that standard 100 ml of water should be allowed to drip, from a height of 400 mm, onto the test block sloped at 1/2 (approximately at 27°). The 100 ml of water dripping should occur during a time interval of 20 to 60 min. The depth of the erosion pit, created by the water dripping impact, should be assessed along with the depth of water penetration into the block (by breaking the block immediately after the test ends).

For the present study, adaptations were made to the NZS procedure (NZS 2000) because the plaster specimens are significantly thinner than the earthen blocks defined in the NZS standard and, in this study, the water erosion effect was intended to also be evaluated through the assessment of the amount of material lost by the specimens during the test. The amount of water to be dripped was reduced proportionally to the 15 mm thickness of plaster samples, being limited to 12 ml. The dripping time was reduced to an interval of 2.4 to 3.0 min corresponding to a water flow interval of 4 to 5 ml/min, which is similar to the maximum flow allowed by the NZS standard (NZS 2000). The specimen positioning slope was increased to 2/1

(approximately at 63°) to emphasize the material lost by the specimens due to water erosion "run off" effect, which barely does not occur with the NZS set (NZS 2000) that promotes mostly water erosion "splash" effect (Pennock 2019). Therefore, a specimen support was specifically made with a metal mesh to allow the loose material to flow out of the specimen. Figure 2 presents a diagram of the apparatus prepared for this test and an earth-based plaster specimen being tested that shows a significant material loss.

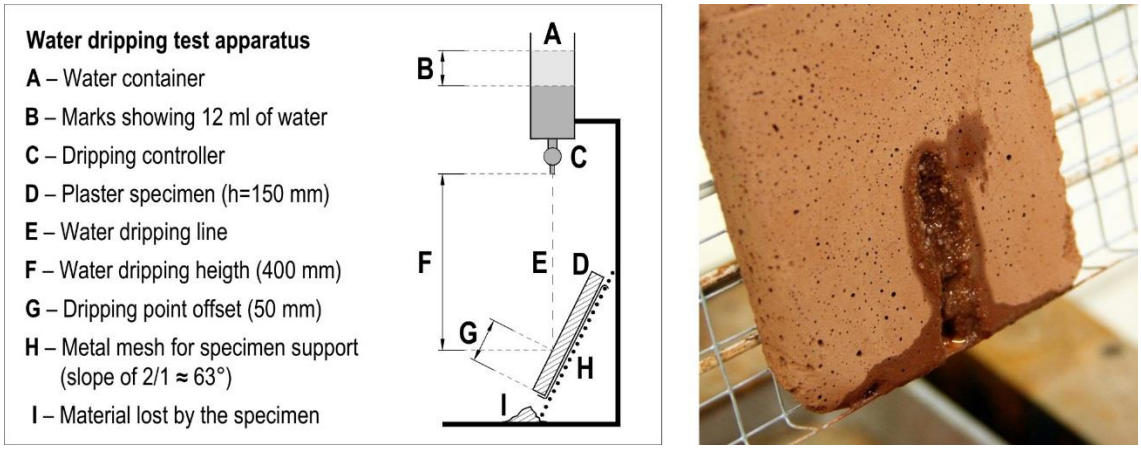

Figure 2. Apparatus for water erosion test by dripping action, adapted from NZS 4298 (NZS 2000): apparatus diagram (left); detail of an earth-based plaster specimen being tested showing significant material loss (right).

2.2.9. Pore size distribution

The pore size distribution test was performed with a mercury intrusion porosimeter (MIP) Micromeritics Autopore IV. The test starts with mercury intrusion at low-pressure, ranging from 0.01 MPa to 0.21 MPa, followed by high-pressure intrusion from 0.28 to 206.84 MPa allowing equilibration times of 15 s for low pressure and 30 s for high-pressure range. The following mercury parameters were considered: advancing and receding contact angle of 140°; surface tension of 0.485 N/m, and density of 13.5335 g/cm³.

The MIP test was carried out with specimens taken from the planar samples, which were prepared in metallic moulds for the dynamic adsorption and desorption test and, therefore, were

not subject to the influence of the substrate. The specimens were sized to occupy most of the 5 cm^3 volume of the penetrometer bulb and were stabilized at 60 °C until achieving constant mass. Similar test procedures are commonly followed for lime mortar testing (Grilo et al. 2014).

3. Results and discussion

3.1. Mineralogical composition

Table 2 summarizes the mineralogical composition of the earthen materials assessed by XRD, which confirms a mineralogical composition dominated, respectively, by illite (earth E), kaolinite (clay K), and montmorillonite (earth B). It should be noted that in clayish earth E, quartz is also a predominant compound while dolomite and kaolinite are also detected in medium proportions along with small amounts of iron oxide (hematite). In clay K, apart from kaolinite predominance, small amounts of illite, quartz, hematite, and feldspar were detected. In montmorillonitic clayish earth B, feldspar was also detected in medium proportion.

Table 2. Mineralogical composition of the clayish earths assessed by XRD.

Crystalline compounds	Clayish materials		
	E	K	B
Magnesiohornblende($Ca_2[Mg_4(Al,Fe^{+++})]Si_7AlO_{22}(OH)_2$)	–	–	tr
Dolomite ($CaMg(CO_3)_2$)	+/++	–	–
Feldspar ($(K,Na,Ca)AlSi_3O_8$)	?	+	++
Gibbsite ($Al(OH)_3$)	–	tr	–
Hematite (Fe_2O_3)	+	+	–
Kaolinite ($Al_2Si_2O_5(OH)_4$)	+/++	+++	–
Montmorillonite ($(Na,Ca)_{0.3}(Al,Mg)_2Si_4O_{10}(OH)_2 \bullet n(H_2O)$)	–	–	++/+++
Muscovite/illite ($KAl_2Si_3AlO_{10}(OH)_2$)	++/+++	+	–
Quartz (SiO_2)	++/+++	+	–

Notation: +++, high proportion (predominant compound); ++, medium proportion; +, low proportion; tr, traces; –, undetected; ?, doubts in presence.

Figure 3 presents the TG-DTG curves of the three clayish earths. The TG-DTG curves agree with the mineralogical composition obtained (Table 2), showing characteristic weight loss patterns for the clay types assessed.

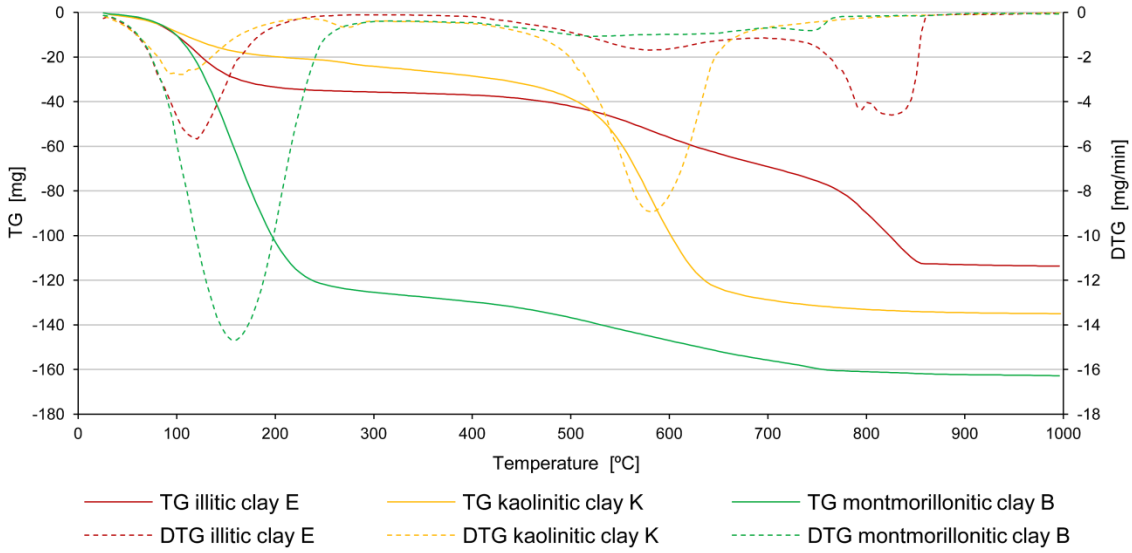

Figure 3. Thermogravimetric (TG) and derivative thermogravimetric curves (DTG).

The first important weight loss occurs at relatively low temperature, until 200 ºC for illitic clayish earth E and kaolinitic clay K and until 250 ºC for montmorillonitic clayish earth B, corresponding to the release of free or sorbed water (Bernal et al. 2017). The second weight loss phase occurs at mid-range temperature, from 400 ºC to 650 ºC, for illitic clayish earth E and kaolinitic clay K and continues until 750 ºC for montmorillonitic clayish earth B, corresponding to the loss of bounded water or dissociation of hydroxyls from the lattice, inducing its amorphization (Bernal et al. 2017). At high temperature, from 750 ºC to 850 ºC, ensues the final breakdown of the residual clay lattice and eventual formation of new mineral and/or glass phases (Bernal et al. 2017). For illitic clay E, this happens along with decarbonation of dolomite present in this earthen material in medium proportion.

3.2. Loose bulk density and particle size distribution

The loose bulk density of the three clayish materials reflects its origin. The illitic clayish earth (E) and montmorillonitic clayish earth (B), both corresponding to excavated natural soils (mechanically ground to pass through a 2 mm sieve), respectively, presented a loose bulk density of 1317 and 1066 kg/m^3, denoting balanced composition of clay, silt, and sand. The

kaolinitic clay (K), quarried in a clay pit (supplied in powder form ground to pass through a 30 μm sieve), showed a loose bulk density of 393 kg/m^3 in accordance with the declared high concentration of clay (MIBAL 2005). The differences of loose bulk densities justify the differences on weight ratios obtained for the mortars – from Table 1, 1:3.6, 1:12.2, and 1:4.5, respectively, for E1S3, K1S3, and B1S3.

The sand S, used for the formulation of all the mortars, presented a loose bulk density of 1592 kg/m^3, and Figure 4 presents its particle size distribution analysed by dry sieving according to standard EN 1015–1 (CEN 1998a).

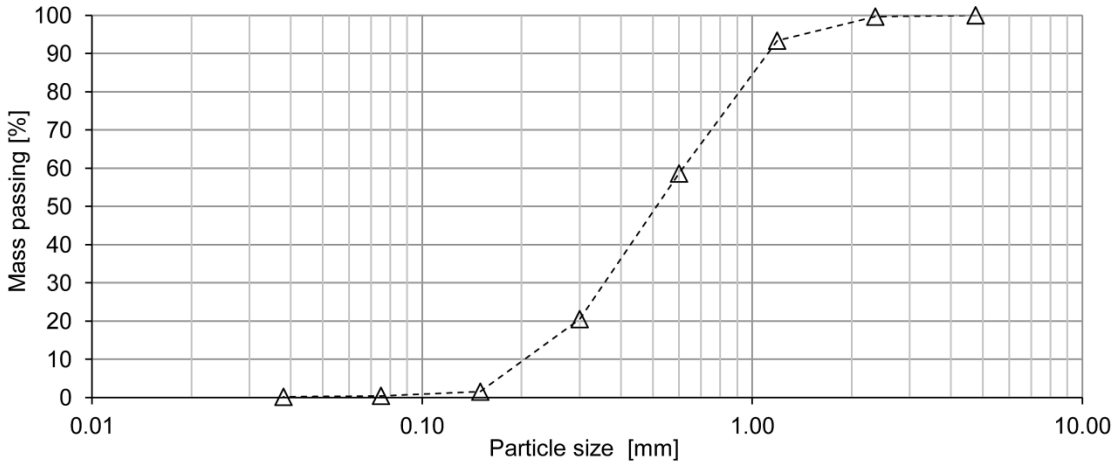

Figure 4. Particle size distribution curve of sand S by dry sieving.

3.3. Linear drying shrinkage

Mortars linear drying shrinkage was assessed on the prismatic samples as well as on the planar samples. The results obtained on both types of samples reflect the mortars clayish earth mineralogy and are presented in Figure 5(A). Kaolinitic mortar K1S3 presents the lowest shrinkage (0.38% for prismatic samples) while montmorillonitic mortar B1S3 shows the highest shrinkage at a rate almost 10 times higher (3.30% for prismatic samples). Illitic mortar E1S3 presents an intermediate shrinkage value, although relatively low and closer to kaolinitic mortar (0.85% for prismatic samples). The correlation between linear drying shrinkage of

prismatic and planar samples (Figure 5B) reveals that both types of samples show similar shrinkage behaviour. However, it is important to note that for low shrinkage mortars, like K1S3, the difference between the shrinkage of these types of samples can be significant (mortar K1S3 presents a ratio of 73.4%).

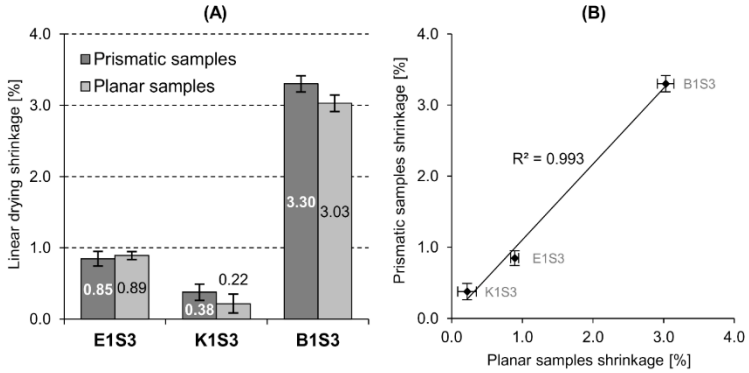

Figure 5. (A) Linear drying shrinkage assessed in prismatic and planar samples; (B) Prismatic sample shrinkage vs. planar sample shrinkage.

Figure 6 presents the samples of 20 mm plaster layer applied over hollow bricks. The occurrence of plaster cracking is significant on montmorillonitic mortar B1S3, rare on illitic mortar E1S3, and absent on kaolinitic mortar K1S3, in accordance with the results of the linear drying shrinkage test and also reflects each mortar clayish earth mineralogy.

Figure 6. Samples of 20 mm plaster layer applied over hollow bricks: (A) Illitic mortar; (B) Kaolinitic mortar; (C) Montmorillonitic mortar.

3.4. Apparent dry bulk density and thermal conductivity

Figure 7(A) presents the results of apparent dry bulk density and thermal conductivity tests. The illitic mortar E1S3 presents the higher bulk density, which falls within density class 2.0 as defined in DIN 18947 (DIN 2013) and is similar to results obtained by the authors in previous campaigns (Lima and Faria 2016; Lima, Faria, and Santos Silva 2016) and other researchers that also study not stabilized illitic mortars (Santos, Faria, and Silva 2019; Santos, Nunes, and Faria 2017). The kaolinitic and montmorillonitic mortars, K1S3 and B1S3, present similar values of bulk density, which are slightly lower than the illitic mortar E1S3, falling within density class 1.8 of the standard previously mentioned, and are also within the interval range of the results assessed by other researchers that studied mortars with similar composition and mineralogy (Delinière et al. 2014; Gomes, Faria, and Gonçalves 2018). In the previous research that studied mortars formulated with different ratios of clayish earth and siliceous sand (Lima and Faria 2016), the authors found a correlation between bulk density and drying shrinkage. That correlation is not clearly present in this study results (Figure 7B), which emphasizes the influence of clay mineralogy in earth-based plaster properties.

Regarding thermal conductivity, the illitic and kaolinitic mortars, E1S3 and K1S3, present almost equal results, which are within the same range of the results found in other studies (Gomes, Faria, and Gonçalves 2018; Lima and Faria 2016; Lima, Faria, and Santos Silva 2016). In comparison, the montmorillonitic mortar B1S3 shows a relatively lower thermal conductivity (less 27%) although with similar dry bulk density of mortar K1S3. These results evidence that thermal conductivity does not follow the trend of bulk density results (Figure 7B), which contradicts the correlation found by the authors in previous campaigns (Lima and Faria 2016; Lima, Faria, and Santos Silva 2016) and by other researchers (Laborel-Préneron, Magniont, and Aubert 2018; Santos, Nunes, and Faria 2017). These results again highlight the influence of clay mineralogy in earth-based plaster performance.

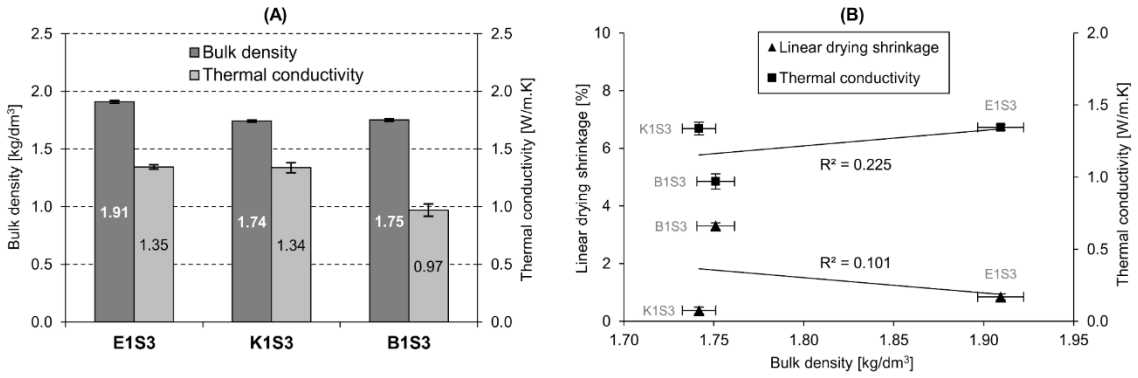

Figure 7. (A) Apparent bulk density and thermal conductivity; (B) Apparent bulk density vs. linear drying shrinkage and vs. thermal conductivity.

3.5. Compressive, flexural and adhesive strength, and dynamic modulus of elasticity

Figure 8(A) shows the results of compressive, flexural, and adhesive strength along with dynamic modulus of elasticity. Illitic mortar E1S3 obtained the higher values of compressive and flexural strength, however, not achieving (by a small difference) the minimum values of mechanical strength defined in the resistance class S-I of the DIN 18947 (DIN 2013) (compressive strength ≥1.0 MPa and flexural strength ≥0.3 MPa). The kaolinitic and montmorillonitic mortars, K1S3 and B1S3, obtained significantly lower compressive and flexural strengths, the latter presenting slightly higher values.

Only mortar E1S3 achieved the minimum values of adhesion strength defined in the resistance class S-I of the DIN 18947 (DIN 2013): ≥0.05 MPa. Again, mortars K1S3 and B1S3 show significantly lower adhesion strength; in this case, the latter presents the lowest value. Adhesion strength, like linear drying shrinkage, is an extremely important property for plastering mortars and, once more, these results highlight the influence of the clays.

The results of dynamic modulus of elasticity show that illitic mortar E1S3 has the higher value, montmorillonitic mortar B1S3 the lowest value, and kaolinitic mortar K1S3 an intermediate value. When correlating dynamic modulus of elasticity with compressive and flexural strength (Figure 8B), no significant concordance is observed. This result is different

from what is usually considered for earthen materials as mentioned by other researchers (Gomes, Faria, and Gonçalves 2018) and some standards (NZS 2000). Nevertheless, a strong correlation is evidenced between dynamic modulus of elasticity and adhesive strength (R^2 = 0.901). Because this tendency is not followed by any other results of the tests performed in this study, neither by the ratios of clayish earth and sand present in mortar formulations (Table 1), it seems likely it may be driven also by clay mineralogy.

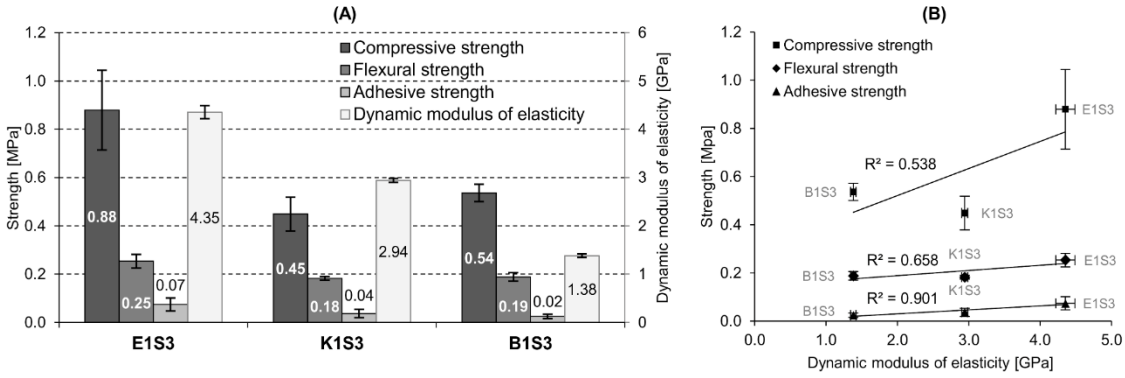

Figure 8. (A) Compressive, flexural, and adhesive strength and dynamic modulus of elasticity; (B) Dynamic modulus of elasticity vs. compressive, flexural, and adhesive strength.

3.6. Dry abrasion resistance

Figure 9 presents the mortar samples surface aspect after dry abrasion test. Abrasion test results are expressed by the mass loss of the tested samples and are presented in Figure 10(A). It can be observed that illitic mortar E1S3 is significantly more resistant to dry abrasion than the other two mortars, and kaolinitic mortar K1S3 is by far the less resistant.

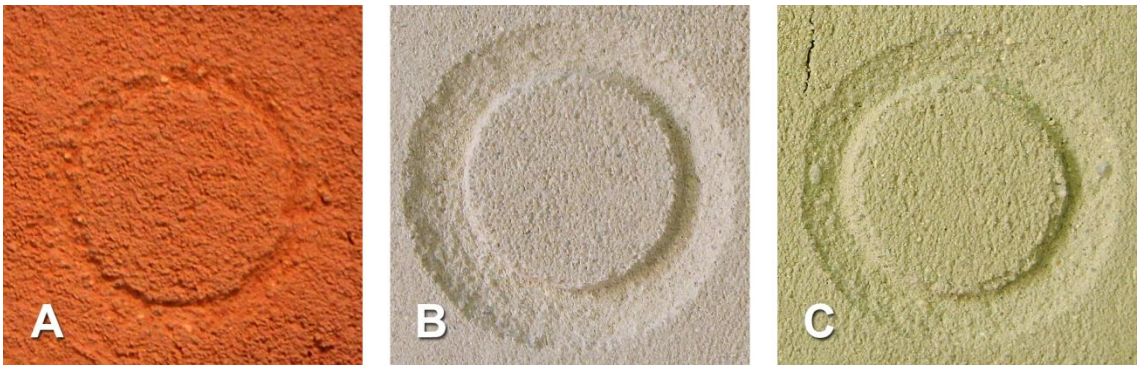

Figure 9. Aspect of dry abrasion on samples of 20 mm plaster layer applied on hollow bricks: (A) - Illitic mortar; (B) - Kaolinitic mortar; (C) - Montmorillonitic mortar.

To some extent, a negative correlation between dry abrasion resistance and mortar mechanical strength is observed (Figure 10B). This negative concordance is particularly evident regarding dry abrasion and compressive strength (R^2 = 0.957), being also strong with flexural strength (R^2 = 0.894) and less significant with adhesive strength. In real-world applications, plaster dry abrasion resistance is one of the properties of utmost importance directly influencing plaster lifecycle. These results seem to indicate that, as previously mentioned for mechanical strength, clay mineralogy is a key factor also for dry abrasion resistance.

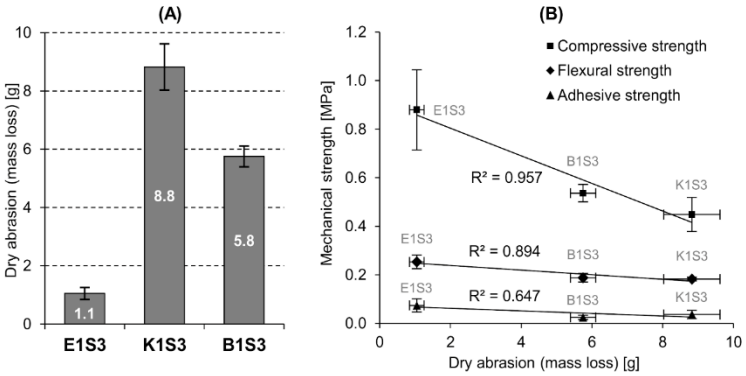

Figure 10. (A) Dry abrasion (mass loss); (B) Dry abrasion (mass loss) vs. compressive, flexural, and adhesive strength.

3.7. Dynamic vapour adsorption and desorption

Plasters' vapour adsorption and desorption capacity is of utmost importance because it allows

the plasters to act as a moisture buffer, passively contributing to balance the RH of the indoor environment of buildings and, therefore, benefits energy saving and sensitive material conservation and promotes comfort and health of inhabitants.

The results of the dynamic vapour adsorption and desorption test are presented in Figure 11 along with the limits of the three adsorption classes defined in DIN 18947 (DIN 2013). The montmorillonitic plaster B1S3 shows a very high adsorption and desorption capacity, achieving a significant vapour adsorption of 110 g/m^2 after 12 h, which is almost the double of class WS-III (≥60 g/m^2). In comparison, illitic plaster E1S3 presents lower values although still showing a high adsorption and desorption capacity slightly above the same class WS-III. In turn, kaolinitic plaster K1S3 obtained the lowest adsorption and desorption capacity with adsorption after 12 h near class WS-I (≥35 g/m^2).

These results clearly show that vapour adsorption and desorption of earth-based plaster is significantly driven by clay mineralogy, reflecting the high hygroscopicity of montmorillonite clay mineral, the low hygroscopicity of kaolinite, and the intermediate behaviour of illite. Nevertheless, it should be noted that vapour adsorption and desorption is also dependent on the mortar clay contents. Although the data of the present study do not provide for an analysis of that correlation, such relationship was demonstrated by the authors in a previous study specifically addressing the correlation between illitic mortars with diverse clay contents to its adsorption capacity (Lima, Faria, and Santos Silva 2016).

While having significantly diverse vapour adsorption capacity, in terms of adsorption and desorption pattern, the three plasters exhibit similar dynamic behaviours. However, it should be noted that montmorillonitic plaster B1S3 and illitic plaster E1S3 present some desorption hysteresis, both with a similar value of 8%. Similar hysteresis effect was found in previous studies comprising illitic mortars (Lima and Faria 2016; Lima, Faria, and Santos Silva 2016). In the present study, kaolinitic plaster K1S3 does not present any hysteresis effect.

It is important to note the significance of vapour adsorption and desorption capacity of earth-based plasters and its contribution to passively balancing the RH of the indoor environment of buildings. Considering a small building compartment with floor dimensions of 3 m x 3 m, with a ceiling height of 3 m, with a window of 1 $m^{2,}$ and a door of 2 m^2, having the walls and ceiling coated with the illitic plaster E1S3 of 15 mm thickness, if indoor RH variation occurs ranging from 50% to 80%, a plaster adsorption capacity of almost 2 kg of vapour is expected after 6 h.

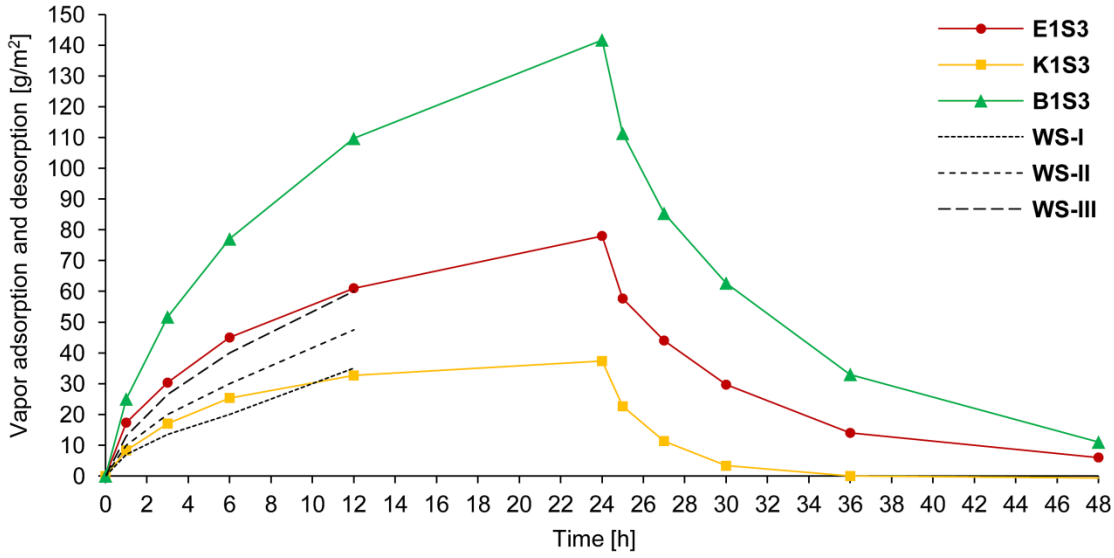

Figure 11. Vapour adsorption and desorption of plasters and vapour adsorption classes defined in DIN 18947 (WS-I, WS-II, and WS-III).

3.8. Water absorption by capillarity action and drying behaviour

The curves of water absorption by capillarity are presented in Figure 12(A) along with linear regression equations and coefficients of determination for the segments selected as most representative of capillary water absorption coefficients (AC). Figure 12(B, C) presents the drying curves plotted, respectively, as a function of time (h) and as a function of square root of the time ($h^{1/2}$), along with linear regression equations and coefficients of determination for the segments selected as most representative of the drying rate (D_1) and rate of water vapour

diffusion (D_2) of, respectively, in the first and the second drying phases. The mortars capillary coefficient AC, drying rate D_1, and vapour diffusion rate D_2, as well as the corresponding standard errors and coefficients of determination are summarized in Table 3.

The results show that the montmorillonitic mortar B1S3 presents significantly higher AC than the other mortars (2.01 $kg/m^2/min^{0.5}$) and higher total absorbed water (asymptotic value). Kaolinitic mortar K1S3 and illitic mortar E1S3 show lower and relatively close AC, with K1S3 presenting 0.34 $kg/m^2/min^{0.5}$, more than the double AC value of E1S3 (0.15 $kg/m^2/min^{0.5}$) although absorbing a similar total amount of water. Mortars E1S3 and B1S3 show similar drying behaviour during the first drying phase (0.17 $kg/m^2/h$), while mortar K1S3 present a slightly lower drying rate (0.15 $kg/m^2/h$). During the second drying phase, a distinct mortar behaviour can again be observed, similar to what was observed in the capillarity test but less pronounced. In this phase Montmorillonitic mortar B1S3 shows the higher vapour diffusion rate (1.13 $kg/m^2/h^{0.5}$), followed by kaolinitic mortar K1S3 (0.97 $kg/m^2/h^{0.5}$), while illitic mortar E1S3 presents the lowest vapour diffusion rate (0.88 $kg/m^2/h^{0.5}$). Note that all mortar achieved equilibrium with room condition at barely the same time (10 days). Mortar B1S3, despite the higher AC and similar D_1, achieved equilibrium at the same time due to the higher D_2. Mortars K1S3 and E1S3, that presented a similar total amount of absorbed water, achieved equilibrium also at the same time, due to mortar K1S3, although presenting a slightly lower D_1, showing D_2 slightly higher. No clear correlations were found between the mortars' capillary and drying behaviour and the other properties of the mortars assessed in this study. Moreover, note can be made regarding the illitic mortar E1S3 that, although presenting the lower D_2 on the drying test, it obtained an intermediate, and relatively high, vapour adsorption in the dynamic vapour adsorption test previously discussed, which may be related to mortar vapour permeability of the mortar. Nevertheless, to some extent, the observed capillary and drying behaviour can be considered related to mortar pore size distribution discussed later in section 3.10.

These results are not directly comparable with the work of other researchers due to specificities of materials used by each mortar's formulation and testing procedures. Some comparison can be pointed with Faria, Santos, and Aubert (2016) that found relatively higher AC and D_1 values for illitic-kaolinitic mortars, respectively, 0.50 kg/m^2/min$^{0.5}$ and 0.30 kg/m^2/h, which tested with equivalent procedures. Gomes, Faria, and Gonçalves (2018) also found higher AC value (0.31 kg/m^2/min$^{0.5}$) although with lower D_1 value (0.08 kg/m^2/h) for an illitic mortar and significantly higher AC value for a kaolinitic mortar (1.08 kg/m^2/min$^{0.5}$) although with a similar and D_1 value (0.13 kg/m^2/h).

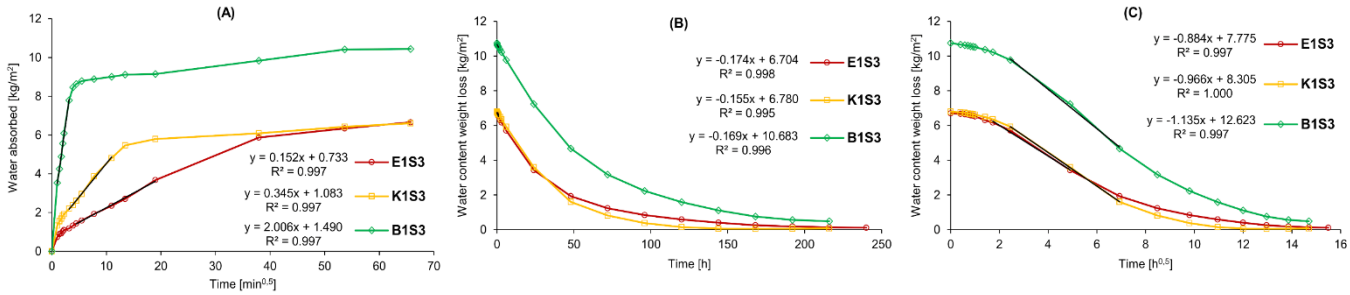

Figure 12. (A) Capillarity curves of water absorbed along with linear regression equations and coefficients of determination of capillarity coefficient; (B) Drying curves, plotted as function of time (h), along with linear regression equations and coefficients of determination of drying rate of first drying phase; (C) Drying curves, plotted as function of square root of the time (h$^{0.5}$) along with linear regression equations and coefficients of determination of drying rate of second drying phase.

Table 3. Capillary water absorption coefficient and drying rates of the first and the second drying phases.

Mortar	Water absorption by capillarity			Drying phase 1			Drying phase 2		
	AC	SE	R^2	D_1	SE	R^2	D_2	SE	R^2
	[kg/m^2/min$^{0.5}$]	[kg/m^2/min$^{0.5}$]	[–]	[kg/m^2/h]	[kg/m^2/h]	[–]	[kg/m^2/h$^{0.5}$]	[kg/m^2/h$^{0.5}$]	[–]
E1S3	0.15	0.00	0.9967	0.17	0.00	0.9984	0.88	0.05	0.9965
K1S3	0.34	0.01	0.9965	0.15	0.01	0.9953	0.97	0.01	0.9999
B1S3	2.01	0.05	0.9973	0.17	0.01	0.9963	1.13	0.06	0.9969

Notation: AC, capillary water absorption coefficient; D_1, drying rate of the first drying phase; D_2, rate of water vapour diffusion of the second drying phase; SE, standard error of the regression lines; R^2, coefficient of determination of the regression lines.

3.9. Water erosion by dripping action

Figure 13 presents the eroded aspect of a dried sample of each mortar submitted to water erosion by dripping action test. The test results are expressed by the mass loss and water absorbed by the specimen during the test, presented in Figure 14(A), as well as, expressed by the area of the impact zone (caused by water dripping "splash" effect), and by impact zone maximum depth showed on Figure 14(B). It is observed that kaolinitic mortar K1S3 suffered more than the double mass loss (21.3 g) when compared with illitic mortar E1S3 (9.2 g) and montmorillonitic mortar B1S3, which presented the lower mass loss (7.7 g). Mortars K1S3 and B1S3 present a similar amount of absorbed water during the test, respectively, 5.4 and 5.0 g, while mortar E1S3 absorbed significant lower amount of water (3.1 g). Regarding the area of the impact zone, mortar E1S3 presents a slightly small impact area (289.6 mm^2) while mortars K1S3 and B1S3 obtained closer results of impact area (respectively, 332.1 mm^2 and 343.2 mm^2). Concerning the impact zone maximum depth, it is noticeable that mortar B1S3 shows significant higher impact depth (12.7 mm), barely achieving the total thickness (15.0 mm). Mortars E1S3 and K1S3 obtained equal results for impact depth (7.5 mm).

Because no clear correlations were found between the water erosion test results and the other properties of the mortars assessed in this study, these results seem to be driven by clay mineralogy, particularly for mortars E1S3 and B1S3. The results of mortar K1S3 may also be influenced by mortar clay-sand ratio, the lowest among the three mortars studied, which may promote lack of mortar cohesion justifying the higher mass loss, mostly caused by the water erosion "run off" effect, that occurred on the edge of the specimens, rather than by the "splash" effect that occur in the impact zone (Figure 13B).

Although the erosion test methodology followed in this study was based on the "Geelong test" defined in NZS 4298:1998/A1 (NZS 2000), due to the extensive test adaptions made the obtained results are not comparable with previous studies.

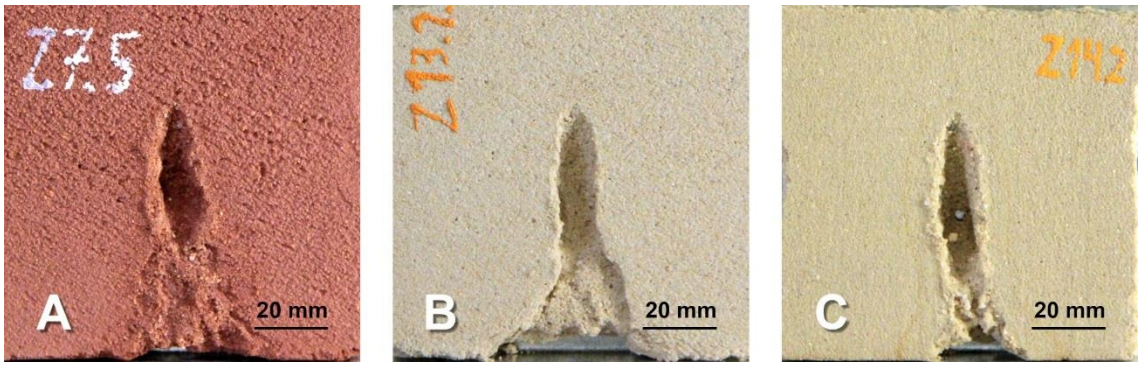

Figure 13. Aspect of water erosion by dripping action samples after drying: (A) Illitic mortar E1S3; (B) Kaolinitic mortar K1S3; (C) Montmorillonitic mortar B1S3.

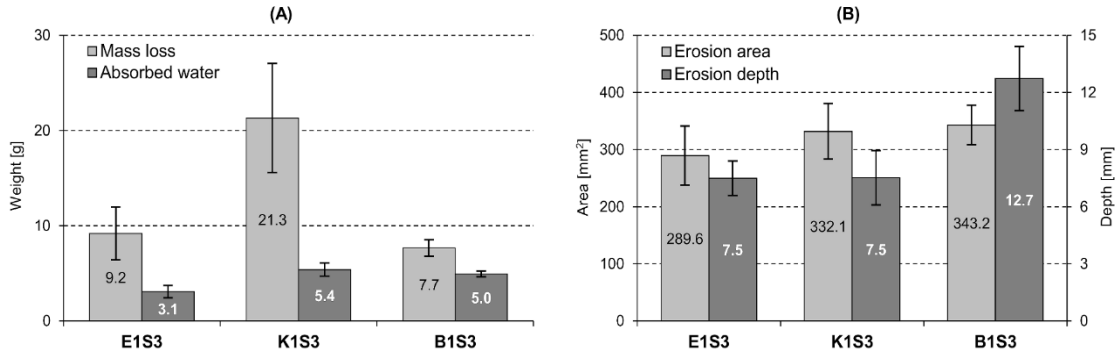

Figure 14. Water erosion by dripping action: (A) Mass loss and water absorbed; (B) Impact zone erosion area and depth.

3.10. Pore size distribution

Incremental mercury intrusion curves for specimens taken from the planar samples, as previously mentioned, prepared in metallic moulds and thus not subject to the substrate influence, are plotted for the whole pore range in Figure 15(A) and only for the lower part of the pore range in Figure 15(B). The pore size diameter is expressed in microns and each step of the mercury intrusion is in millilitres per gram.

It is observable that illitic mortar E1S3 and kaolinitic mortar K1S3 present almost the same microstructure along the whole pore range, showing the most frequent pore diameter ranging from 80 to 100 μm with differential mercury intrusion of approximately of 0.02 mL/g.

An exception is observed for 8 to 10 µm, pore range where E1S3 shows slightly higher pore frequency. It is mentionable that these mortars were prepared with relatively different earth-added sand mass ratios; therefore, a more distinct microstructure was expected. In turn, montmorillonitic mortar B1S3, although prepared with earth-sand mass ratio closer to mortar E1S3, demonstrates clearly a distinct pore distribution, presenting the most frequent pore diameter ranging around 50 µm with a differential mercury intrusion of slightly higher than of 0.04 mL/g, nearly the double of the differential intrusion obtained by the other two mortars at its most frequent pore diameter range. On the lower part of the pore range (Figure 15B) mortars K1S3 and E1S3 continue to present quite similar pore distribution, with closer peaks of differential mercury intrusion (slightly higher than of 0.002 mL/g), ranging around pore diameter 0.1 and 0.2 µm, respectively. However, at this lower part of the pore range, montmorillonitic mortar B1S3 do not present relevant pore diameter frequency. These low-diameter pore range results again do not follow the earth-sand mass ratios considered in mortars preparation, highlighting the influence of clay mineralogy in mortars microstructure.

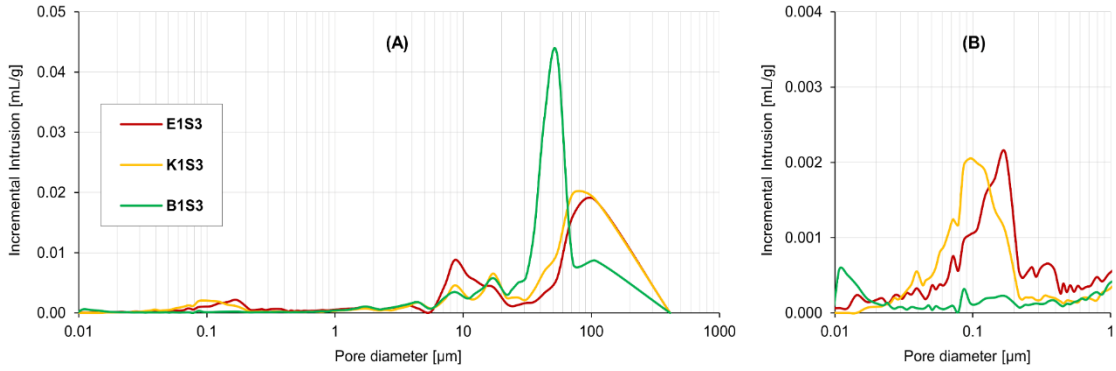

Figure 15. Incremental mercury intrusion curves: (A) pore diameter range from 0.01 to 1000 µm; (B) pore diameter range from 0.01 to 1.0 µm.

Table 4 presents the mortar results regarding bulk density, open porosity, and total pore area assessed in the MIP test. The mortars apparent dry bulk density results assessed geometrically following EN 1015–10 (CEN 1999b), previously presented, differ, although not substantially,

from the bulk density results obtained in the MIP test. Figure 16(A) shows that, despite the results slight difference, a correlation is observed between both test methods. Figure 16(B) highlights that a correlation is found between open porosity and thermal conductivity; however, it should be noted that mortars E1S3 and K1S3 present closer values. Figure 16(C) presents the observed correlation between mortars total pore area and vapour adsorption capacity, noting that the mortar microstructure, which seems to be driven by clay mineralogy, also drives the mortar vapour adsorption capacity.

Table 4. Bulk density, open porosity, and total pore area, assessed by MIP.

Mortar	Bulk density[(A)] [kg/dm³]	Open porosity [%]	Total pore area [m²/g]
E1S3	2.22	26.5	1.28
K1S3	2.09	25.8	1.19
B1S3	2.05	33.9	1.61

Notation: (A) Assessed at 0.53 psia (absolute pressure).

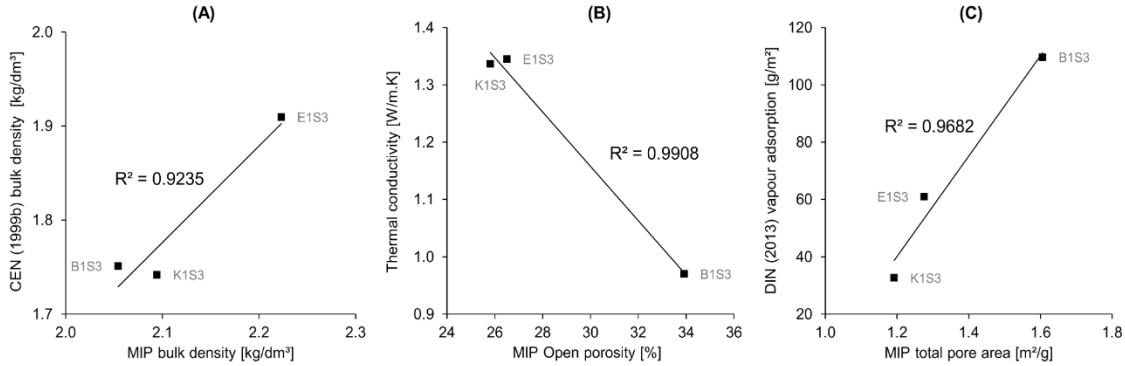

Figure 16. (A) Apparent bulk density vs. bulk density assessed by MIP; (B) Open porosity assessed by MIP vs. thermal conductivity; (C) Total pore area assessed by MIP vs. vapour adsorption.

4. Conclusions

The findings of this study allow to conclude that clay mineralogy plays a key role in the properties of the earth-based plasters assessed in this study. It clearly drives vapour adsorption and desorption capacity, water capillary absorption, linear dry shrinkage, and shrinkage

cracking, and has a significant influence on mechanical strength, dry abrasion, thermal conductivity, drying behaviour, and pore size distribution, although with less obvious interpretation.

Among the studied mortars, the illitic clayish earth stands outs as more adequate to produce earth-based plasters, presenting an advantageous balance between plaster key properties, like linear drying shrinkage, mechanical strength, dry abrasion, vapour adsorption and desorption, water erosion by dripping action, and capillary and drying behaviour.

To allow a more comprehensive knowledge of the role clay mineralogy may have in the performance of earth-based plasters, more research is necessary as to its influence on mortar vapour permeability, as well as the eventual interaction of clay minerals with different types of sand with diverse particle size and mineralogy.

The demand for water required by each mortar during its preparation to achieve the desired consistency range and workability should also be comprehensively studied, seeing that water added during mixing is also influencing the mortars' properties. The study of particle size distribution of the fine fraction of the illitic and montmorillonitic clayish earths and the assessment of their Atterberg limits will provide more insight into this matter. Both should be included in future studies.

Efforts should also be made to better understand what drives the dynamic vapour adsorption and desorption hysteresis effect presented by the montmorillonitic and illitic plasters. The desorption delay of plaster can generate a lag effect between consecutive cycles of adsorption and desorption, which, over a certain period of time, may lead to a decrease of adsorption and desorption capacity of the plaster or even to its full moisture saturation.

5. Funding

The authors acknowledge the support of Fundação para a Ciência e a Tecnologia (FCT), Portugal, for funding José Lima's scholarship (SFRH/BD/119703/2016), as well as the research project PTDC/EPH-PAT/4684/2014: DB-Heritage - Database of building materials with historical and heritage interest.

6. Acknowledgments

The authors acknowledge the EMBARRO company for providing the illitic clayish earth, the MIBAL mining company for providing the kaolin clay for this study and Mary Barros-Bailey for the text review.

7. Disclosure statement

No potential conflict of interest was reported by the authors.

8. ORCID

José Lima – http://orcid.org/0000-0002-1377-8570

Paulina Faria – http://orcid.org/0000-0003-0372-949X

António Santos Silva – https://orcid.org/0000-0001-8002-0682

9. References

Bergaya, F., and G. Lagaly, eds. 2013. Handbook of clay science – Part A: Fundamentals, vol. 5. Amsterdam: Elsevier. Developments in Clay Science.

Bernal, S. A., M. C. G. Juenger, X. Ke, W. Matthes, B. Lothenbach, N. De Belie, and J. L. Provis. 2017. Characterization of supplementary cementitious materials by thermal analysis. Materials and Structures 50 (26):1–13. doi:10.1617/s11527-016-0909-2.

Bruno, P., P. Faria, A. Candeias, and J. Mirão. 2010. Earth Mortars from pre-historic habitat settlements in South Portugal: Case studies. Journal of Iberian Archaeology 13:51–67.

CEN. 1998a. EN 1015-1:1998 – methods of test for Mortar for Masonry; Part 1: Determination of particle size distribution (by Sieve analysis). Brussels, Belgium: CEN. European Standard.

CEN. 1998b. EN 1015-6:1998 – methods of test for Mortar for Masonry. Part 6: Determination of bulk density of fresh mortar. Brussels, Belgium: CEN. European Standard.

CEN. 1998c. EN 1097-3:1998 – tests for mechanical and physical properties of aggregates - Part 3: Determination of loose bulk density and voids. Brussels, Belgium: CEN. European Standard.

CEN. 1999a. EN 1015-3:1999 – methods of test for mortar for masonry; Part 3: Determination of consistence of fresh mortar (by Flow Table). Brussels, Belgium: CEN. European Standard.

CEN. 1999b. EN 1015-10:1999 – methods of test for masonry; part 10: Determination of dry bulk density of hardened mortar. Brussels, Belgium: CEN. European Standard.

CEN. 1999c. EN 1015-11:1999 – methods of test for masonry; part 11: Determination of flexural and compressive strength of hardened mortar. Brussels, Belgium: CEN. European Standard.

CEN. 2000. EN 1015-12:2000 – methods of test for mortar for masonry; part 12: Determination of adhesive strength of hardened rendering and plastering mortars on substrates. Brussels, Belgium: CEN. European Standard.

CEN. 2004. EN 14146:2004 – natural stone test methods. Determination of the dynamic modulus of elasticity (By measuring the fundamental resonance frequency). Brussels, Belgium: CEN. European Standard.

CEN. 2009. EN 15801:2009 – conservation of cultural property - test methods - determination of water absorption by capillarity. European Standard. Brussels, Belgium: CEN.

CEN. 2013. EN 16322:2013 – conservation of cultural heritage - test methods - determination of drying properties. Brussels, Belgium: CEN. European Standard.

Cordeiro, N., J. Silva, C. Gomes, and F. Rocha. 2010. Bentonite from Porto Santo Island, Madeira Archipelago: Surface properties studied by inverse gas chromatography. Clay Minerals 45 (1):77–86. doi:10.1180/claymin.2010.045.1.77.

Delinière, R., J. E. Aubert, F. Rojat, and M. Gasc-Barbier. 2014. Physical, mineralogical and mechanical characterization of ready-mixed clay plaster. Building and Environment 80:11–17. doi:10.1016/j.buildenv.2014.05.012.

DIN (German Institute for Standardization). 2013. DIN 18947: 2013-08– Earth plasters – Terms and definitions, requirements, test methods (in German). Berlin: DIN.

Emiroğlu, M., A. Yalama, and Y. Erdoğdu. 2015. Performance of ready-mixed clay plasters produced with different clay/sand ratios. Applied Clay Science 115:221–29. doi:10.1016/j.clay.2015.08.005.

Faria, P., T. Santos, and J.-E. Aubert. 2016. Experimental characterization of an earth eco-efficient plastering mortar. Journal of Materials in Civil Engineering 28 (1):04015085. doi:10.1061/(ASCE)MT.1943-5533.0001363.

Gomes, M. I., P. Faria, and T. D. Gonçalves. 2018. Earth-based mortars for repair and protection of rammed earth walls. Stabilization with mineral binders and fibers. Journal of Cleaner Production 172:2401–14. doi:10.1016/j.jclepro.2017.11.170.

Grilo, J., P. Faria, R. Veiga, A. Santos Silva, V. Silva, and A. Velosa. 2014. New natural hydraulic lime mortars – physical and microstructural properties in different curing conditions. Construction and Building Materials 54:378–84. doi:10.1016/j.conbuildmat.2013.12.078.

Laborel-Préneron, A., C. Magniont, and J.-E. Aubert. 2018. Hygrothermal properties of unfired earth bricks: Effect of Barley Straw, Hemp Shiv and Corn Cob addition. Energy and Buildings 178:265–78. doi:10.1016/j.enbuild.2018.08.021.

Lagouin, M., A. Laborel-Préneron, C. Magniont, and J.-E. Aubert. 2019. Development of a high clay content earth plaster. IOP Conference Series: Materials Science and Engineering 660:012068. doi:10.1088/1757-899X/660/1/012068.

Lima, J., and P. Faria. 2016. Eco-efficient earthen plasters: The influence of the addition of natural fibers. In Natural fibres: Advances in science and technology towards industrial applications, ed. R. Fangueiro, and S. Rana, Vol. 12, 315–27. Dordrecht: Springer Netherlands. doi: 10.1007/978-94-017-7515-1_24.

Lima, J., P. Faria, and A. Santos Silva. 2016. Earthen plasters based on illitic soils from barrocal region of algarve: Contributions for building performance and sustainability. Key Engineering Materials 678:64–77. doi:10.4028/www.scientific.net/KEM.678.64.

Manuppella, G., B. Moreira, C. Grade, and C. Moura. 1985. Contribuição para o conhecimento das características das argilas do Algarve. In Estudos, Notas e Trabalhos. Tomo, Vol. 27, 59–75. Porto: Serviço de Fomento Mineiro e Laboratório da D.G.G.M.

Maskell, D., A. Thomson, P. Walker, and M. Lemke. 2018. Determination of optimal plaster thickness for moisture buffering of indoor air. Building and Environment 130:143–50. doi:10.1016/j.buildenv.2017.11.045.

MIBAL (Mibal Minas de Barqueiros S.A). 2005. Product Data Sheet – Kaolin MIB-A. Barqueiros, Portugal: Mibal Minas de Barqueiros S.A.

Minke, G. 2006. Building with earth: Design and technology of a sustainable architecture. 6th ed. Basel, Boston: Birkhauser-Publishers for Architecture.

Murray, H. 2007. Applied clay mineralogy: Occurrences, processing and application of kaolins, bentonites, palygorskite-sepiolite, and common clays, vol. 2. Amsterdam: Elsevier. Developments in Clay Science.

NZS (New Zealand Standards). 2000. NZS 4298:1998/A1:2000 Materials and workmanship for earth buildings. Wellington, New Zealand: New Zealand Standard: NZS.

Pennock, D. 2019. Soil erosion: The greatest challenge for sustainable soil management. Rome: FAO – Food and Agriculture Organization of the United Nations.

Santos, I., C. Costa, A. Quintela, D. Terroso, E. Ferraz, F. Rocha, O. Dorzhieva, V. Krupskaya, and M. Vigasina. 2014. Mineralogical composition of sedimentary and residual Kaolin deposits from Portugal. Comunicações Geológicas 101 (1):195–97.

Santos, T., P. Faria, and V. Silva. 2019. Can an earth plaster be efficient when applied on different masonries? Journal of Building Engineering 23:314–23. doi:10.1016/j.jobe.2019.02.011.

Santos, T., L. Nunes, and P. Faria. 2017. Production of eco-efficient earth-based plasters: Influence of composition on physical performance and bio-susceptibility. Journal of Cleaner Production 167:55–67. doi:10.1016/j.jclepro.2017.08.131.

Schroeder, H. 2016. Sustainable building with earth. Cham, Switzerland: Springer International Publishing. doi:10.1007/978-3-319-19491-2.

Trindade, M., F. Rocha, M. Dias, and M. Prudêncio. 2013. Mineralogy and grain-size distribution of clay-rich rock units of the algarve basin (South Portugal). Clay Minerals 48 (1):59–83. doi:10.1180/claymin.2013.048.1.04.

White, W. A., and E. Borrelli. 1959. Water-sorption characteristics of clay minerals. Illinois, USA: Illinois State Geological Survey (ISGS).